

The monogenic signal of potential-field data: A Python implementation

Marlon C. Hidalgo-Gato¹ and Valéria C. F. Barbosa²

ABSTRACT

We have developed codes to calculate the local amplitude, the local phase, and the local orientation of the nonscale and the Poisson's scale-space monogenic signals of potential-field data in version 1.0 of the open-source program Monogenic. The monogenic vector of a generic function is calculated in the wavenumber domain and then transformed back into the space domain to find the monogenic signal attributes. We compare the use of the nonscale monogenic signal with the Poisson's scale-space monogenic signal in magnetic data. This comparison shows that the latter can produce better results as an edge detection filter. The implementation of the monogenic signal can be used to enhance other geophysical data, such as seismic, ground-penetrating radar, gravity, multiple-component gravity gradiometry, and magnetic gradient data.

INTRODUCTION

Most edge detection filters in geophysical applications are based on the derivative of the field. One of the most popular filters is the 2D analytical signal proposed by Nabighian (1972). The 2D analytical signal is the amplitude of the vector composed by the horizontal and vertical derivatives of the data. Nabighian (1984) introduces the 3D analytical signal, and Roest et al. (1992) propose the total gradient. The total gradient is the amplitude of the vector composed by the x - and y -horizontal derivatives and the vertical derivative of the data. Gradient amplitude-based filters fail to enhance strong and weak anomalies simultaneously. On the other hand, the tilt angle (Miller and Singh, 1994) enhances weak and strong anomalies produced by shallow- and deep-seated sources equally well.

One of the biggest problems of edge detection filters based on derivatives, and especially the ones that use vertical derivatives, is the enhancement of the noise content. Because of this, Hassan and Yalamanchili (2013) propose the monogenic signal attributes of magnetic data as a set of filters based on the Riesz transform that do not use only the derivative of the data. The monogenic signal is an image-processing tool proposed by Felsberg and Sommer (2001) that can be applied to any kind of image data. In contrast with the classic edge detection filters used in geophysical applications, the monogenic signal is applied directly to the data and does not require derivatives. Cooper (2014) proposes the zero-order analytical signal, which in practice is the same as the amplitude of the monogenic signal proposed by Hassan and Yalamanchili (2013). Following Felsberg and Sommer's (2001) approach, Hidalgo-Gato and Barbosa (2015) propose the Poisson's scale-space monogenic signal of a potential-field function as an edge detection filter. In this paper, we refer to the monogenic signal attributes presented by Hassan and Yalamanchili (2013) as the nonscale monogenic signal. In what follows, we refer to the scale-space monogenic signal presented by Hidalgo-Gato and Barbosa (2015) as the Poisson's scale-space monogenic signal.

The nonscale and the Poisson's scale-space monogenic signals are 3D vectors composed of the data and its first-order Riesz transform. The nonscale monogenic signal uses the original data, whereas the Poisson's scale-space monogenic signal uses the Poisson's scale-space representation of the original potential-field data. Hidalgo-Gato and Barbosa (2015) show that the Poisson's scale-space monogenic signal has better performance as an edge detection filter than the nonscale monogenic signal. The latter can produce smoothed or misshapen contacts of the bodies.

In this paper, we present the Python 2.7/3.5 program Monogenic to calculate the nonscale and the Poisson's scale-space monogenic signal attributes based on the definitions introduced by Hidalgo-Gato and Barbosa (2015). In addition, we make available the Python script "synthetic.py" and the data "data.dat" to run our synthetic test example.

Peer-reviewed code related to this article can be found at <http://software.seg.org/2017/0002>.

Manuscript received by the Editor 25 February 2016; revised manuscript received 8 October 2016; published online 06 March 2017.

¹Observatório Nacional, Rio de Janeiro, Brazil and CGG Multi-Physics, Rio de Janeiro, Brazil. E-mail: marlonchg@hotmail.com; marlon.cabrera@cgg.com.

²Observatório Nacional, Rio de Janeiro, Brazil. E-mail: valcris@on.br.

© 2017 Society of Exploration Geophysicists. All rights reserved.

BUILDING THE POISSON'S SCALE-SPACE MONOGENIC VECTOR

The Poisson's scale-space monogenic signal of a potential-field function $f(x, y)$, which is measured in a constant height ($z = \text{constant}$), is a 3D vector given by

$$\mathbf{m}(x, y) = \begin{bmatrix} f_{bp} \\ r_{xp} \\ r_{yp} \end{bmatrix}, \quad (1)$$

where $f_{bp} \equiv f_{bp}(x, y)$ is the Poisson's scale-space representation of the original function $f(x, y)$ filtered by a band-pass filter (Felsberg and Sommer, 2001) and $r_{xp} \equiv r_{xp}(x, y)$ and $r_{yp} \equiv r_{yp}(x, y)$ are, respectively, the x - and y -components of the first-order Riesz transform of f_{bp} .

From the Poisson's scale-space monogenic vector (equation 1), we can define the following quantities in the 3D space: (1) the local amplitude:

$$A(x, y) = \sqrt{r_{xp}^2 + r_{yp}^2 + f_{bp}^2}, \quad (2)$$

(2) the local phase:

$$\varphi(x, y) = \tan^{-1} \left(\frac{\sqrt{r_{xp}^2 + r_{yp}^2}}{f_{bp}} \right), \quad (3)$$

and (3) the local orientation:

$$\theta(x, y) = \tan^{-1} \left(\frac{r_{yp}}{r_{xp}} \right) \quad (4)$$

Taking the Fourier transform of the Poisson's scale-space monogenic vector (equation 1), Hidalgo-Gato and Barbosa (2015) show that the Fourier transform of each components is a 3D vector given by

$$\mathcal{M}(u, v) = \begin{bmatrix} p \cdot F \\ i \frac{u}{\sqrt{u^2 + v^2}} \cdot p \cdot F \\ i \frac{v}{\sqrt{u^2 + v^2}} \cdot p \cdot F \end{bmatrix}, \quad (5)$$

where u and v are the wavenumbers in the x - and y -directions, respectively, $F \equiv F(u, v)$ is the Fourier transform of the potential-field data $f(x, y)$, $i = \sqrt{-1}$ and $p \equiv p(h_c, h_f, u, v)$ is a band-pass filter that maps the original function into the Poisson's scale-space representation, being defined as

$$p = \left(e^{-2\pi h_f \sqrt{u^2 + v^2}} - e^{-2\pi h_c \sqrt{u^2 + v^2}} \right), \quad (6)$$

where $h_c > h_f > 0$ are the parameters related to the Poisson's scale-space representation (Felsberg and Sommer, 2001).

Alternatively, the nonscale monogenic signal can be constructed from equation 5 by setting $p = 1$. In this particular case, the three components of the monogenic signal will be given by the original data function, and its first-order Riesz transform; i.e.,

$$\mathcal{M}_{\text{NS}}(u, v) = \begin{bmatrix} F \\ i \frac{u}{\sqrt{u^2 + v^2}} F \\ i \frac{v}{\sqrt{u^2 + v^2}} F \end{bmatrix}. \quad (7)$$

INSIDE THE MONOGENIC SIGNAL

In equations 5 and 7, iu and iv are the filters that transform a function $f(x, y)$ measured on a horizontal surface into first-order derivatives with respect to the x - and y -directions, respectively. As pointed out by Hidalgo-Gato and Barbosa (2015), these terms enhance the high-wavenumber contents. Nonetheless, if $f(x, y)$ is a potential-field function, then the filter $1/\sqrt{u^2 + v^2}$ transforms this function into its first-order vertical integration, which attenuates the high-wavenumbers amplitudes. In addition, note that the filter p in equation 6 represents a band-pass filter given by the difference between two upward-continuation filters at different observation levels controlled by the parameters h_c and h_f . The combination of a band-pass filter and the vertical integral transformation of a potential-field function makes the local amplitude, the local phase, and the local orientation in the Poisson's scale-space monogenic signal less sensitive to noise than regular filters such as the total gradient (Roest et al., 1992) and tilt angle (Miller and Singh, 1994).

We understand that a band-pass filter may attenuate and/or completely remove some signal wavelengths. The choice of the parameters h_c and h_f (equation 6) is done by trial and error to band pass the wavelengths related to the noise contents. The best values of these parameters will depend on the grid dimensions and the noise level of the data. In practice, we verified that a good initial approximation for these parameters can be given by fixing h_c close to the grid spacing and setting h_f to approximately 10% less than h_c .

As compared with the Poisson's scale-space monogenic signal, the nonscale monogenic signal (equation 7) is easier to use because it does not require tuning of the Poisson's parameters (h_c and h_f in equation 6) to band-pass filter the data. In fact, the nonscale monogenic signal (equation 7) uses the original data only. However, in enhancing the weak magnetic responses of deep sources, the nonscale monogenic signal can distort the boundaries of the sources. In this paper, we present the open-source codes of both functions: (1) the nonscale monogenic signal and (2) the Poisson's scale-space monogenic signal in the wavenumber domain.

COMPUTATIONAL DETAILS

We have implemented codes to calculate the local amplitude, the local phase, and the local orientation of the nonscale monogenic signal and the Poisson's scale-space monogenic signal in version 1.0 of the open-source program Monogenic. The code was implemented in Python 2.7/3.5 language and is executed using Anaconda2 64 bit. The Anaconda Python is a freely available package that includes the NumPy library, which is necessary to run the code. However, you may run the code in any other Python 2.7 interpreter as long as the NumPy library is installed. Our code is freely available online (<http://software.seg.org/2017/0002>) under the Berkeley Software Distribution three-clause open-source license. Alternatively, all accompanying material is available in an online repository (Hidalgo-Gato and Barbosa, 2017).

In the program Monogenic v 1.0, we present two functions: (1) `nss_monogenic_signal(x, y, data, pad_pt, and pad_mode)` and

(2) `pss_monogenic_signal(x, y, data, hc, hf, pad_pt, and pad_mode)`, where x and y are the 2D arrays containing the north–south and east–west coordinates, the data are a 2D array with the potential-field data to be transformed, hc and hf are the scalars required by the Poisson’s scale-space monogenic signal (equation 6), and `pad_pt` and `pad_mode` are the parameters used to set the data padding. The choice of padding parameters will be discussed later. If the Poisson’s scale-space parameters are passed to the `pss_monogenic_singal` function as `None` ($h_c = h_f = \text{None}$), then the monogenic code will automatically calculate default values following our recommendations. Both functions return the local amplitude, the local phase, and the local orientation of a 2D array. Equations 2–4 express these attributes in the case of the Poisson’s scale-space monogenic vector.

In our algorithm, we assume a regular grid at a constant height observation level ($z = \text{constant}$). For a computational convenience, our algorithm calculates the three components of the monogenic signal vector in the wavenumber domain and then transforms it back into the space domain. Finally, we calculate the local amplitude, local phase, and the local orientation of the monogenic signal.

The algorithm of both functions (`nss_monogenic_signal` and `pss_monogenic_signal`) inside the file “`monogenic.py`” is summarized in the following pseudocode:

Function `monogenic_signal`

Input $\leftarrow \begin{cases} x = \text{north coordinates} \\ y = \text{east coordinates} \\ \text{data} = \text{input data} \end{cases}$

- pad the data
- calculate the fast Fourier transform
- calculate the Fourier wavenumbers
- calculate the x - and y -components of the first-order Riesz transform
- transform the data and the Riesz components back into the space domain
- remove the pad
- calculate the local amplitude, local phase, and local orientation.

Output $\rightarrow \begin{cases} \text{local amplitude} \\ \text{local phase} \\ \text{local orientation} \end{cases}$

Note that the two components of the first-order Riesz transform in the wavenumber domain (equations 5 and 7) have a singularity point $(0, 0)$. For this reason, we zero out the DC frequency of the Riesz components of the monogenic signal vector. On the other hand, equation 6 is also zero at point $(0, 0)$. This is the same as removing a constant averaged value of the data, and it makes the scale-space monogenic signal attributes independent of the DC component. The fast Fourier transform (FFT) package inside the NumPy library was used to transform the data in the wavenumber domain and calculate the Fourier wavenumbers.

Data padding

To avoid edge effects using the fast Fourier transform, we extend the 2D data array. We have included a padding function to expand the data using three different modes: linear ramp, edge, and mean values. The pad is included in both monogenic signal functions, and the user can specify the mode (`mode`) and the number of points (`pad_pt`) to expand the 2D array.

The linear ramp mode (`linear_ramp`) pads the data with a linear ramp between zero and the edge values. This padding function will always fill the edges of the padded array with zeros. The edge mode (`edge`) fills all the padded area with the values of the closer edges, whereas the mean values mode (`mean`) pads with the mean values of each rows and columns.

The number of padding points (`pad_pt`) to be added to the original data array in all directions is an integer number. For example, for an original data array of 2×2 points and a `pad_pt = 2`, the extended data array will have dimensions of 6×6 given by

$$\begin{bmatrix} 4 & 9 \\ 7 & 6 \end{bmatrix} \Rightarrow \text{padding with line arramp} \Rightarrow \begin{bmatrix} 0 & 0 & 0 & 0 & 0 & 0 \\ 0 & 1 & 2 & 4 & 2 & 0 \\ 0 & 2 & 4 & 9 & 4 & 0 \\ 0 & 4 & 7 & 6 & 3 & 0 \\ 0 & 2 & 4 & 3 & 2 & 0 \\ 0 & 0 & 0 & 0 & 0 & 0 \end{bmatrix}. \quad (8)$$

Note that, in this example, we padded the array with a linear ramp mode; thus, the values are decreasing to zero without changing the center of the original data array. Big data expansions will increase the computation time and may cause overflow. We performed some synthetic tests using the three padding modes with different `pad_pt` values. Our simulations show that a small number of padding points is sufficient to avoid edge effects without affecting the computer memory and processing time.

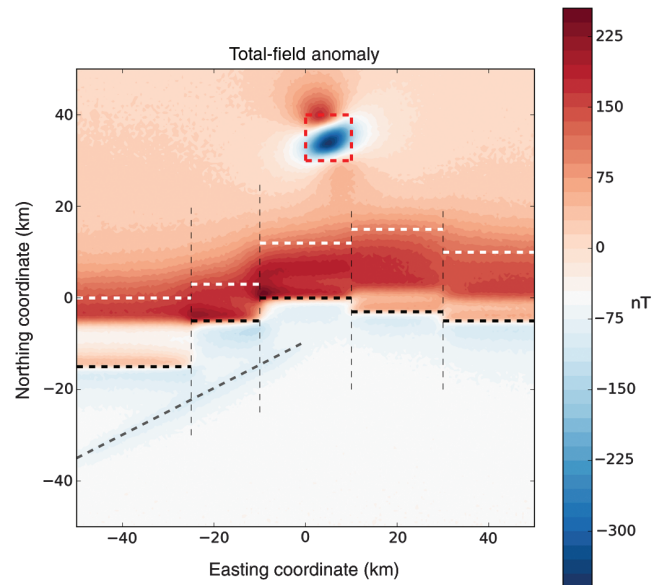


Figure 1. Synthetic test. Noise-corrupted total-field anomaly produced by the geologic model of Figure 2. The horizontal dashed lines are the projection in the horizontal plane of the hinge line (black), continental oceanic boundary (white), and the edges of the igneous intrusion and the dike (gray). The vertical dashed lines are the transfer zones between displacements in the basement.

After padding the data, we transform it to the wavenumber domain and calculate the Riesz components. Each Riesz component and the data in the Poisson's scale-space are then transformed back into the space domain. Finally, we remove the pad restoring the data array to its original size before calculating the monogenic signal attributes.

SYNTHETIC MODEL APPLICATION

Figure 1 shows the computed noise-corrupted total-field anomaly produced by a simulated passive margin basin. The 3D synthetic model (Figure 2) illustrates a crustal thinning geologic set. It is possible to identify some geologic features, such as the hinge line (dashed black line), the continental oceanic boundary (COB) (white dashed line), an igneous intrusion in the middle of the oceanic crust (dashed red lines), and a dike cutting the shallow basement in the continental crust (dashed gray line). The top of the dike is located at a 1500 m depth from the top of the basement.

The magnetic basement is uniformly magnetized by induction with an intensity of 1.5 A/m in continental crust and 2.5 A/m in oceanic crust. The igneous intrusion and the dike are also magnetized by induction with an intensity of 2.8 A/m. All the geologic

bodies were magnetized with an inclination of -10° and a declination of -20° . We assume that there is no magnetization above the basement. The edges of the geologic structures were extrapolated constantly to avoid strong magnetic anomalies near the edges.

By using the implementation of Uieda et al. (2013), we calculate the total-field anomaly produced by the geologic model shown in Figure 2 at -100 m height on a regular grid of 200×200 observation points in the north-south and east-west directions leading to grid spacing of 500 m along both directions. The magnetic anomaly was then corrupted with pseudorandom zero-mean Gaussian noise with a standard deviation of 2.5 nT.

The x -, y -, and z -coordinates (in meters) and the noise-corrupted total-field anomaly (in nT) were exported to an ASCII file named data.dat. The Python script synthetic.py that accompanies this paper has the following structure: (1) open the data file, (2) calculate the monogenic signal attributes, and (3) plot the maps. In addition to the NumPy library, the Matplotlib is also required to run the script synthetic.py. In addition, we padded the original data using the linear ramp mode adding 10 points (pad_pt) in all directions before computing the fast Fourier transform. We tested all three pad modes implemented and concluded that all of them work well. In our tests, we use only 10 padding points that correspond to 5% of the data points in one direction of the grid.

Figures 3a–3c and 4a–4c show the local amplitude, the local phase, and the local orientation of, respectively, the nonscale and the Poisson's scale-space monogenic signals applied to the total-field anomaly (Figure 1). To calculate the Poisson's scale-space monogenic signal, we used $h_c = 500$ m and $h_f = 450$ m. Note that we used h_c close to the input grid spacing and h_f 10% less than h_c as recommended before. The horizontal dashed lines are the projection in the horizontal plane of the hinge line (in black), COB (in white), the edges of the igneous intrusion (in red), and the dike (in gray). The dashed vertical lines are the transfer zones between displacements in the basement.

Our synthetic test simulates three different types of anomalies (Figure 1). The igneous intrusion and the dike clearly produce, respectively,

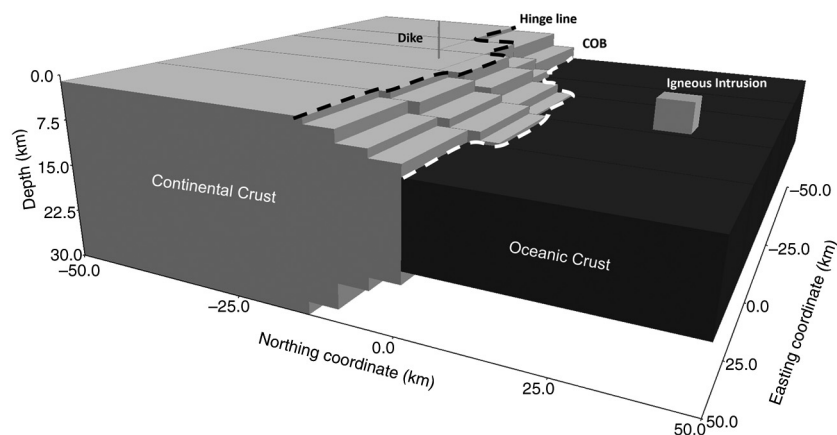


Figure 2. Perspective view of the simulated passive margin model. The dashed lines are the hinge line (black) and the continental oceanic boundary (white).

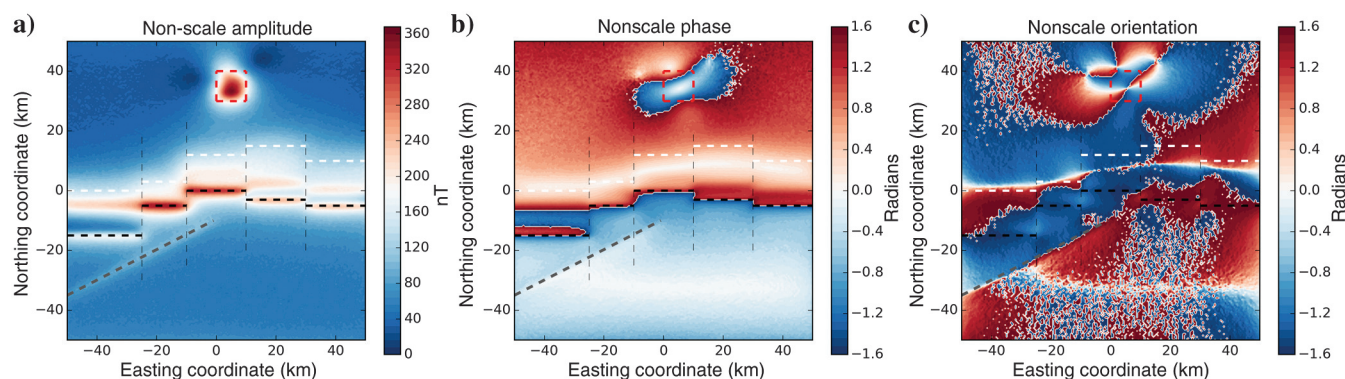


Figure 3. Enhancements of the total-field anomaly of Figure 1 using the (a) local amplitude, (b) the local phase, and (c) the local orientation of the nonscale monogenic signal. The horizontal dashed lines are the projection in the horizontal plane of the hinge line (black), continental oceanic boundary (white), and the edges of the igneous intrusion (red) and the dike (gray). The vertical dashed thin lines are the transfer zones between displacements in the basement.

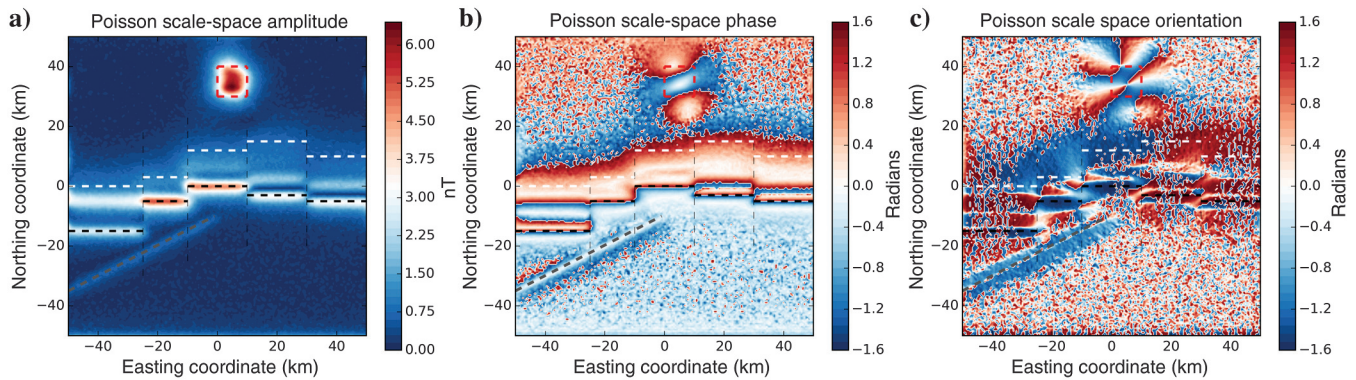


Figure 4. Enhancements of the total-field anomaly of Figure 1 using the (a) local amplitude, (b) the local phase, and (c) the local orientation in the Poisson's scale-space monogenic signal. The horizontal dashed lines are the projection in the horizontal plane of the hinge line (black), continental oceanic boundary (white), and the edges of the igneous intrusion (red) and the dike (gray). The vertical dashed thin lines are the transfer zones between displacements in the basement.

3D and 2D magnetic anomalies. On the other hand, the hinge line and the COB produce signals that can be locally approximated by 2D magnetic anomalies.

Note that neither the nonscale (Figure 3) nor the Poisson's scale-space monogenic signal (Figure 4) is able to enhance the edges of the igneous intrusion because the magnetization vector is not vertical and the intrusion produces a 3D magnetic anomaly. On the other hand, the 2D anomaly produced by the dike is very well-enhanced using the monogenic signal attributes even in the case of a nonvertical magnetization vector. These results are expected because, as shown by Hidalgo-Gato and Barbosa (2015), the enhancement of 2D magnetic anomalies with the monogenic signal does not require a vertical magnetization vector. Rather, in case of 3D magnetic anomalies the magnetization vector must be vertical to enhance the true boundaries of the source by using the monogenic signal.

Taking into account these results, one might think that the monogenic signal of a nonvertical magnetization source can only be used to enhance 2D magnetic anomalies. However, we note that even locally 2D magnetic anomalies such as the hinge line and the COB highlighted in Figures 1 and 2 can be enhanced using the monogenic signal attributes in the presence of nonvertical magnetization.

The main difference between the nonscale and the Poisson's scale-space monogenic signal is that the amplitude and phase of the latter produces sharper contacts, as shown in Figures 3 and 4. The most striking feature of the local phase in the Poisson's scale-space monogenic signal (Figure 4b) is that it enhances the edges of the dike, the hinge line, and the COB better than the local phase in the nonscale monogenic signal (Figure 3b).

As shown in Figures 3c and 4c, the local orientation of the monogenic signal of a potential field function has not produced a meaningful enhancement of any features of the geologic sources.

CONCLUSION

We have presented the program Monogenic, a Python 2.7/3.5 package of two functions to calculate the nonscale and the Poisson's scale-space monogenic signals of a 2D data. Both monogenic signal functions return the local amplitude, the local phase, and the local orientation of a potential-field data or any kind of 2D array. Compared with the Poisson's scale-space monogenic signal, the nonscale monogenic signal is easier to use because the former

requires band-pass filtering the data, whereas the nonscale monogenic signal requires only the original data set. However, the Poisson's scale-space monogenic signal yields a sharper image of boundaries of the geologic bodies than the nonscale monogenic signal. We demonstrated the use of the monogenic signal by applying it to synthetic magnetic data. The Python script `synthetic.py` contains the algorithm to run our synthetic example. This example was run using specific Poisson's scale-space parameters. However, users can try different Poisson's scale-space parameters for the same synthetic model. Finally, we stress that the application of the nonscale and the Poisson's scale-space monogenic signals to enhance other geophysical data (e.g., seismic, ground-penetrating radar, gravity, multiple-component gravity gradiometry, and magnetic gradient data) has no methodological obstacles.

ACKNOWLEDGMENTS

We thank associate editor J. Dellinger, reviewers L. Uieda, T. Irons, and an anonymous reviewer for their criticisms and suggestions that helped to improve the first version of the code. We acknowledge the open-source Python tool kit for geophysical modeling and inversion (Uieda et al., 2013) called *Fatiando a Terra* (Portuguese for Slicing the Earth). V. C. F. Barbosa was supported in this research by a fellowship (grant no. 307135/2014-4) from Conselho Nacional de Desenvolvimento Científico e Tecnológico (CNPq), Brazil. Additional support for V. C. F. Barbosa is provided by Brazilian research agency FAPERJ (grant no. E-26/203.091/2016).

REFERENCES

- Cooper, G. R. J., 2014, Reducing the dependence of the analytic signal amplitude of aeromagnetic data on the source vector direction: *Geophysics*, **79**, no. 4, J55–J60, doi: [10.1190/geo2013-0319.1](https://doi.org/10.1190/geo2013-0319.1).
- Felsberg, M., and G. Sommer, 2001, The monogenic signal: *IEEE Transactions on Signal Processing*, **49**, 3136–3144, doi: [10.1109/78.969520](https://doi.org/10.1109/78.969520).
- Hassan, H. H., and S. V. R. Yalamanchili, 2013, Monogenic signal decomposition: A new approach to enhance magnetic data: 83rd Annual International Meeting, SEG, Expanded Abstracts, 1206–1210.
- Hidalgo-Gato, M. C., and V. C. F. Barbosa, 2015, Edge detection of potential-field sources using scale-space monogenic signal: *Fundamental principles: Geophysics*, **80**, no. 5, J27–J36, doi: [10.1190/geo2015-0025.1](https://doi.org/10.1190/geo2015-0025.1).
- Hidalgo-Gato, M. C., and V. C. F. Barbosa, 2017, Source code repository for “The monogenic signal of potential-field data: A Python Implementation”, <https://github.com/pinga-lab/paper-monogenic-signal>, accessed 14 January 2017.

- Miller, H. G., and V. Singh, 1994, Potential field tilt: A new concept for location of potential field sources: *Journal of Applied Geophysics*, **32**, 213–217, doi: [10.1016/0926-9851\(94\)90022-1](https://doi.org/10.1016/0926-9851(94)90022-1).
- Nabighian, M. N., 1972, The analytical signal of 2D magnetic bodies with polygonal cross-section: Its properties and use for automated anomaly interpretation: *Geophysics*, **37**, 507–517, doi: [10.1190/1.1440276](https://doi.org/10.1190/1.1440276).
- Nabighian, M. N., 1984, Toward a three-dimensional automatic interpretation of potential field data via generalized Hilbert transforms: Fundamental relations: *Geophysics*, **49**, 780–786, doi: [10.1190/1.1441706](https://doi.org/10.1190/1.1441706).
- Roest, W. R., J. Verhoef, and M. Pilkington, 1992, Magnetic interpretation using the 3-D analytic signal: *Geophysics*, **57**, 116–125, doi: [10.1190/1.1443174](https://doi.org/10.1190/1.1443174).
- Uieda, L., V. C. Oliveira, Jr., and V. C. F. Barbosa, 2013, Modeling the earth with Fatiando a Terra: Techniques: 12th Python in Science Conference, SCIPY 2013, Proceedings, 90–96.